Journal of Applied Polymer Science

Synthesis and Characterization of Polystyrene Coated Iron Oxide Nanoparticles and Asymmetric Assemblies by Phase Inversion

Yihui Xie,[1] Rachid Sougrat,[2] Suzana P. Nunes[1]

[1]Water Desalination and Reuse Center, King Abdullah University of Science and Technology, 23955-6900 Thuwal, Saudi Arabia
[2]Imaging and Characterization Lab, King Abdullah University of Science and Technology, 23955-6900 Thuwal, Saudi Arabia
Correspondence to: S. P. Nunes (E-mail: suzana.nunes@kaust.edu.sa)

ABSTRACT: Films with a gradient concentration of magnetic iron oxide nanoparticles are reported, based on a phase inversion membrane process. Nanoparticles with ~13 nm diameter were prepared by coprecipitation in aqueous solution and stabilized by oleic acid. They were further functionalized by ATRP leading to grafted polystyrene brush. The final nanoparticles of 33 nm diameter were characterized by TGA, FTIR spectroscopy, GPC, transmission electron microscopy, and dynanmic light scattering. Asymmetric porous nanoparticle assemblies were then prepared by solution casting and immersion in water. The nanocomposite film production with functionalized nanoparticles is fast and technically scalable. The morphologies of films were characterized by scanning electron microscopy and atomic force microscopy, demonstrating the presence of sponge-like structures and finger-like cavities when 50 and 13 wt % casting solutions were, respectively, used. The magnetic properties were evaluated using vibrating sample magnetometer.
 J. Appl. Polym. Sci. **2015**, *132*, 41368.

KEYWORDS: grafting; membranes; nanoparticles; nanowires and nanocrystals

Received 1 April 2014; accepted 8 July 2014
DOI: 10.1002/app.41368

INTRODUCTION

Ordered nanoparticle assemblies are relevant for nanoelectronic, photovoltaic, optical devices, plasmon absorbance, sensors, and so forth.[1,2] Nanoparticles can self-assemble in packed structures forming 2D monolayers with high order.[3] Collective magnetic properties can be controlled at the nanoparticle level. Nanocrystalline magnetic materials and devices have been constructed and previously reported based on quasi-2D nanoparticles assemblies.[4] Three-dimensional arrangements are much more challenging to manufacture. Polymer-nanoparticle functionalization can help to achieve homogenous dispersion and increase the connectivity between particles as well as the mechanical stability of the assemblies.

Nanoparticle self-assembly in thin films has been investigated by different groups.[6,7] Ohno et al.[5] synthesized monodispersed silica coated with well-defined high-density PMMA brushes. A thin surface film was formed at the air-water interface by depositing one drop of the polymer-grafted silica nanoparticle suspension on the surface of pure water in a Petri dish. Chen Xu et al.[6] investigated the self-assembly of PMMA-grafted magnetite nanoparticles in homopolymer PMMA and lamellar-forming block copolymer PS-b-PMMA films.[6,7] Polymer-grafted nanoparticles and polymers were mixed in solvent. Nanocomposite films were prepared by spin casting and annealing at 185°C. For PS-b-PMMA block copolymer matrice, increasing brush molecular weight drives the magnetite nanoparticles into large aggregates, and the block copolymer assembles into onion-like rings around these aggregates. Uniform dispersion of PMMA-grafted nanoparticles in PMMA copolymer film can be obtained at high brush lengths.

The bulk properties of magnetite (Fe_3O_4) are well-known,[8,9] but nanopartilcles can still show unexpected behavior. Frenkel and Dorfman[10] were for instance the first to predict that a particle of ferromagnetic material, below some critical particle size would be monodomain, i.e. a particle that is a state of uniform magnetization at any field. Because of the very small crystal size and surface effects, magnetic nanoparticles exhibit remarkable new phenomena such as superparamagnetism, high field irreversibility, high saturation field, extra anisotropy contributions and shifted loops after field cooling.[11,12] Iron oxide nanoparticles have potential application in various disciplines, including magnetic seals in motors, magnetic inks for jet printing, data storage, catalysis, and removal of toxic elements from industrial wastes.[13] Especially in biomedical field, many novel applications have been proposed and investigated such as enzyme and

Additional Supporting Information may be found in the online version of this article.

protein immobilization, genes, radiopharmaceuticals, contrast agents for magnetic resonance imaging (MRI), diagnostics for cancer diagnosis, immunoassays, biological labels, RNA and DNA purification, magnetic cell separation, and purification, magnetically-controlled targeted drug carriers as well as magnetic fluid hyperthermia (MFH).[14,15] Nanoengineering assemblies of well-dispersed nanoparticles in macroscopic films might allow to better take advantage of unusual properties observed in nanoparticles and at the same time better integrate them into technological devices.

We propose a new manufacture method for films consisting of a gradient concentration of assembled nanoparticles, inspired by previous work of our group on block copolymer self-assembly membranes.[16,17] Block copolymers assemble into micelles with ordered distribution, when exposed to selective solvent mixtures. When a block copolymer solution layer with controlled concentration is immersed in water, an asymmetric porous structure is formed with interconnected micelles. Here we induce phase separation in a dispersion of polystyrene-functionalized nanoparticles with Fe_3O_4 cores leading to the formation of a film fully constituted by assembled nanoparticles.[16,17]

EXPERIMENTAL

Materials

Ferric chloride hexahyrate ($FeCl_3{\cdot}6H_2O$, ≥99%), ferrous sulfate heptahydrate ($FeSO_4{\cdot}7H_2O$, ≥99%), ammonium hydroxide ($NH_3{\cdot}H_2O$, 28–30%), oleic acid (OA), sodium sulfate (Na_2SO_4, ≥99.0%, anhydrous, powder), toluene (anhydrous, 99.8%), ethanol (absolute, ≥99.8%), γ-aminopropyl triethoxysilane (APTES, ≥98%), triethylamine (TEA, ≥99.5%), *N,N,N′,N″,N″*-pentamethyldiethylenetriamine (PMDETA, 99%), styrene (≥99%), copper(I) bromide (Cu(I)Br, 98%), *N,N*-dimethylformamide (DMF, anhydrous, 99.8%), neutral aluminum oxide (Al_2O_3), sodium hydroxide (NaOH, ≥98%, pellets), tetraoctylammonium bromide (TOAB, 98%), (1-bromoethyl)benzene (97%), deuterated chloroform ($CDCl_3$), and tetrahydrofuran (THF, anhydrous) were purchased from Aldrich Chemical Toluene (laboratory) and methanol (laboratory) were obtained from Fisher Chemical. sodium chloride (NaCl, 99%) and 2-bromoisobutyryl bromide (BiBB, 98%) were supplied by Alfa Aesar and Acros, respectively. Styrene was passed through neutral alumina column to remove inhibitors. All other reagents were used as received.

Synthesis of Oleic Acid (OA) Coated Iron Oxide Nanoparticles

Iron oxide nanoparticles (MNPs) were synthesized by coprecipitation method. First ferric chloride hexahydrate ($FeCl_3{\cdot}6H_2O$) (13.515 g, 0.05 mol) and ferrous sulfate heptahydrate ($FeSO_4{\cdot}7H_2O$) (6.95 g, 0.025 mol) were dissolved into 500 mL deionized water. The as-prepared iron precursor solution was stored at 4°C. In a 250 mL round bottom flask, 100 mL iron precursor solution was magnetically stirred under N_2 protection, followed by adding 20 mL 28–30% (w/w) $NH_3{\cdot}H_2O$ quickly at room temperature. The solution color changed from orange to black, leading to a black precipitate. Then under vigorous stirring, 0.5 mL oleic acid was dropped into the dispersion slowly at 80°C in 1 h. The homogeneous MNPs water dispersion was then mixed with 120 mL toluene in a 500 mL separating funnel. By adding about 10 g of sodium chloride, MNPs transferred into toluene phase with intensively shaking. The resulting toluene based MNPs dispersion was mixed with anhydrous sodium sulfate in a 250 mL Erlenmeyer flask to remove the remaining water. After being desiccated overnight, the supernatant was filtered by a fritted filter funnel (porosity 3) to remove solids with vacuum. Finally, oleic acid coated iron oxide nanoparticles (OA) dispersion was obtained. 20 mL as-synthesized OA-MNP dispersion was precipitated by 20 mL ethanol, followed by magnetic separation. Then, these MNPs were redispersed into toluene and reprecipitated by ethanol. This procedure was repeated three times to remove the excess free OA followed by dried in vacuum at room temperature overnight.

Synthesis of Pristine Iron Oxide Nanoparticles

Hundred-milliliter iron precursor solution was added into a 250 mL round-bottom-flask and magnetically stirred under N_2 protection, followed by adding 20 mL 28∼–30% (w/w) $NH_3{\cdot}H_2O$ quickly at room temperature. The solution color changed from orange to black, leading to a black precipitate. The co-precipitation was carried out in 1 h under vigorous magnetic stirring at 80°°C. This was followed by centrifugation (8000 rpm) and decantation. Then the black product was redispersed into distilled water. The washing procedure was repeated 5 times to remove the remaining excess ions and adjust pH to 7. At last, pristine magnetic nanoparticles powder was obtained by dried under vacuum at room temperature.

Synthesis of Initiator Coated Iron Oxide Nanoparticles

Initiator coated iron oxide nanoparticles were synthesized as illustrated by Figure 1. Hundred milliliter OA-MNPs (∼10 mg/mL) dispersion was transferred into a 250 mL round-bottom-flask, which was connected to a Dean-Stark trap with a condenser on the top. Azeotropic distillation was performed at 140°C oil bath under nitrogen in this setup to remove trace water in iron oxide nanoparticle dispersion. After about 1 h, no more water condensed to the bottom of Dean-Stark trap. Then, APTES (1 mL, 4.27 mmol) was added through syringe. The reaction mixture was kept at 140°C temperature for 12 h under vigorous stirring. The obtained APTES-modified MNPs were precipitated by 100 mL methanol, followed by magnetic separation. Then, these MNPs were redispersed into 100 mL toluene and reprecipitated by methanol. This procedure was repeated 5 times to remove the uncondensed APTES. The obtained amino-functionalized MNPs dispersed in toluene were denoted as NH_2-MNPs Parts of NH_2-MNPs were dried under vacuum for characterization. Thereafter, NH_2-MNPs were used to immobilize the initiator. The procedure is as follows: 100 mL of NH_2-MNPs, triethylamine (0.6 mL, 4.27 mmol), and BiBB (0.53 mL, 4.27 mmol) were placed in a dried 250 mL flask immersed in an ice water bath. The mixture was stirred under nitrogen protection for 3 h at 0°C and then for another 12 h at room temperature. The products bromine coated iron oxide nanoparticles (Br-MNPs) were precipitated by 100 mL methanol, followed by magnetic separation. Then, these MNPs were redispersed into 100 mL toluene and reprecipitated by methanol. This procedure was repeated three times to remove the unreacted BiBB and

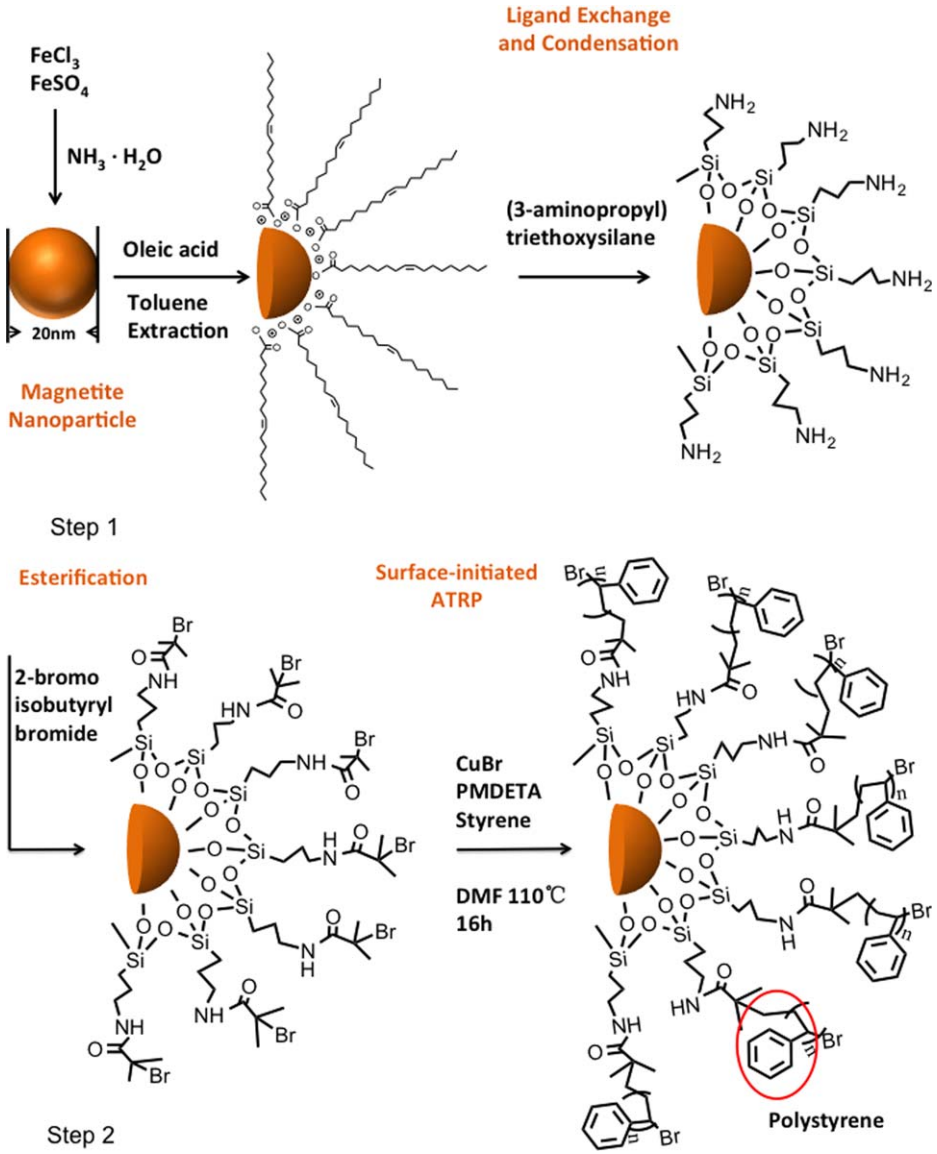

Figure 1. Synthesis route of polystyrene coated nanoparticles (ATRP = atom transfer radical polymerization). [Color figure can be viewed in the online issue, which is available at wileyonlinelibrary.com.]

replaced OA, followed by dried under vacuum at room temperature overnight.

Surface Initiated ATRP on Iron Oxide Nanoparticles

First, to a 25 mL Schlenk tube, 80 mg Br-MNPs powder and 8 mL inhibitor free styrene were added, and the atmosphere was exchanged for N_2. Then the mixture was sonicated for 30 min to make MNPs well dispersed in styrene. Meanwhile, Cu(I)Br (0.057 g, 0.4 mmol), PMDETA (0.084 mL, 0.4 mmol) were dissolved in 1 mL DMF. The mixture was stirred until the homogenous green color was seen. Then, the Cu(I)Br-PMDETA solution was added into the Schlenk tube via syringe. The reactor was immediately degassed by three freeze-pump-thaw cycles with N_2, and then the mixture was stirred in a constant temperature oil bath at 110°C for 16 h. After the polymerization was complete, the polymerization solution was diluted with 200 mL THF and passed through neutral Al_2O_3 column to remove copper catalyst. The filtrate was concentrated by rotary evaporation. The viscous polymer solution was added to 200 mL methanol, and a brown solid precipitated. The solids were isolated by the magnet, and redispersed in THF. Methanol was added to precipitate polystyrene (PS) grafted iron oxide nanoparticles (PS-MNPs), followed by centrifugation (13,000 rpm). The final products PS-MNPs were dried at room temperature under vacuum. PS chains were cleaved from the MNPs as follows: the polymer grafted MNPs (50 mg) were dispersed into 10 mL toluene. The dispersion was mixed with 10 mL 3*M* sodium hydroxide aqueous solution and 50 mg tetraoctylammonium bromide (TOAB) as a phase transfer catalyst. The mixture was vigorously stirred at 60°C for a week to etch the silica surrounding MNPs with strong base. The organic layer was isolated and washed by distilled water several times. Then the solvent was evaporated

by rotary evaporation and dried polymer solids were obtained. Next, the solids were mixed with 100 mL dilute hydrochloric acid (3*M*) and stirred at 40°C for several days to dissolve remaining iron oxide particles, until the color of solids turned from yellow to white. Finally, he cleaved polystyrene was washed by distilled water for several times to adjust pH to 7, dried at 60°C, and then subjected to gel permeation chromatography (GPC) measurement.

ATRP of Pure Polystyrene

First, to a 25 mL Schlenk tube, Cu(I)Br (0.063 g, 0.44 mmol), PMDETA (0.09 mL, 0.44 mmol) and inhibitor free styrene (5 mL, 44 mmol) were added, and the atmosphere was exchanged for N_2. Then, the initiator, (1-bromoethyl)benzene (0.06 mL, 0.44 mmol) was added via syringe. The mixture was stirred in a constant temperature oil bath at 90°C for 130 min. After the polymerization was complete, the solution was diluted with 500 mL THF and passed through neutral Al_2O_3 column to remove copper catalyst. The filtrate was concentrated by rotary evaporation. The viscous polymer solution was precipitated in methanol. Pure polystyrene was obtained after being filtered and then dried at 60°C.

Preparation of Membranes Formed by Nonsolvent Phase Inversion

Two membranes were fabricated from polystyrene coated iron oxide nanoparticles (PS-MNPs). Membrane A was cast from solutions containing 50 wt % PS-MNPs in DMF on a glass plate, using a casting blade with 100 μm gate height. The solvent was allowed to evaporate for 25 s at room temperature, and the film was immersed in a water bath. Finally, the obtained nanocomposite membrane from PS-MNPs and pure polystyrene membrane were dried at ambient conditions. Membrane B was cast using the same nonsolvent phase inversion method, but from 13 wt % NMP solution, with 200 μm gate height and practically no evaporation time.

Characterization

Powder X-ray Diffraction (XRD). Powder X-ray diffraction (XRD) measurement was carried out to characterize the crystal structure of the prestine iron oxide nanoparticles synthesized by coprecipitation. The XRD pattern was recorded using a Bruker D8 Advance diffractometer with Cu Kα radiation source ($\lambda = 1.5406$ Å) at 40 kV and 40 mA. The data were collected from $2\theta = 20°$ to 70° at a step size of 0.01° and a scan speed of 2 s per step.

Dynamic Light Scattering (DLS). Dynamic light scattering (DLS) measurements were taken with a Malvern Zetasizer Nano ZS equipped with a 4 mW solid state He-Ne laser ($\lambda = 633$ nm) at a scattering angle of 173°. Samples of 0.5 mg/mL dispersed in toluene were measured at 20°C using 12 mm square glass cuvettes for the hydrodynamic diameters and size distribution of MNPs.

Fourier Transform Infrared Spectroscopy (FTIR). Fourier transform infrared spectroscopy (FTIR) was performed on a Thermo Nicolet iS10 FT-IR instrument to investigate the chemical structures, in which the spectra were recorded between 400 and 4000 cm^{-1} with 256 scans at a resolution of 0.964 cm^{-1}. The powder samples of iron oxide nanoparticles and polymer were ground with KBr and then compressed into pellets. For liquid samples, a drop of liquid was mixed with KBr and compressed into a pellet.

Thermogravimetric Analysis (TGA). Thermogravimetric analysis (TGA) for the pristine and functionalized iron oxide nanoparticles was monitored using a TA instrument Q50. In a typical procedure, about 6 mg of powder sample was placed into a platinum crucible and heated from 20 to 1000°C, at a heating rate of 5°C/min under a constant flow of nitrogen of 60 mL/min.

Magnetic Characterization

The magnetic properties of MNPs were studied with a Magnetic Property Measurement System (MPMS® SQUID VSM), utilizing Superconducting Quantum Interference Device (SQUID) and vibrating sample magnetometer (VSM). The magnetizations of MNPs were measured as a function of the applied magnetic field between −20,000 Oe and +20,000 Oe at ambient condition.

Gel Permeation Chromatography

Number average molecular weights (M_n), weight average molecular weight (M_w), and polydispersity indices (PDI) of the polystyrene grafted on the iron oxide nanoparticle surface were determined using gel permeation chromatography. GPC were performed at room temperature on a Viscotek GPCmax VE-2001 system consisting of a HPLC pump, one guard column and two LT4000L (pore size 1500 Å) analytical columns (300 × 7.8 mm, particle size 7 μm), Model 305 TDA detectors and Smartline 2600 UV detector. Polymer samples were dissolved in THF at a concentration of 2 mg/mL before being injected into the system. THF was used as a solvent at a flow rate of 1 mL/min. Narrow molecular weight linear polystyrene standard (99 kDa) was used for calibration.

Field Emission Scanning Electron Microscope (FESEM)

The membrane surface and cross section of PS-MNPs nanocomposite membrane were observed on FEI Nova Nano scanning electron microscope (SEM) at 5 kV. For surface imaging, a small piece of membrane sample was mounted on a flat aluminum stub and coated with platinum by sputtering using a K575X Emitech equipment with the duration time of 30 s. The membranes were fractured in liquid nitrogen for cross-section images.

Atomic Force Microscopy (AFM)

AFM was accomplished using an Agilent 5500 SPM AFM operating in tapping mode at ambient conditions to characterize the surface morphology of PS-MNPs membrane. The image was acquired with a Bruker probe in which the nominal spring constant is 2.8 N/m, tip radius is around 10 nm and resonance frequency are 71.27 kHz.

Transmission Electron Microscopy (TEM)

The membrane was embedded in epoxy resin. Ultrathin section (120 nm) were cut and collected on a 3 mm TEM grid. Imaging of samples was performed on a Titan G2 80–300 kV transmission electron microscope (TEM) from FEI Company (FEI Company) equipped with a 4 k × 4 k CCD camera model US4000

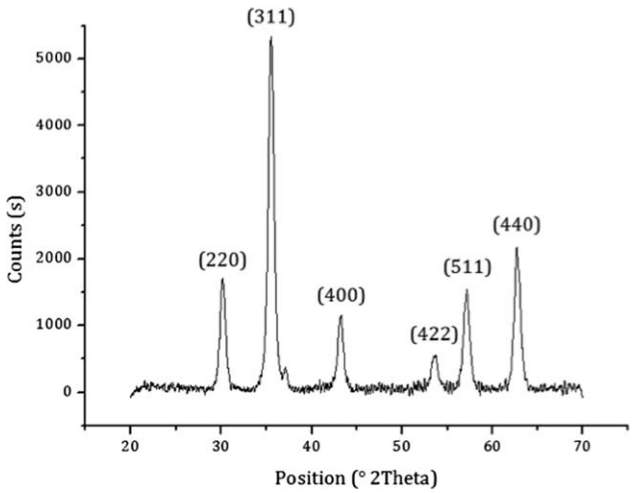

Figure 2. X-ray powder diffraction patterns of the pristine iron oxide nanoparticles.

and an energy filter model GIF Tridiem (Gatan). Electron energy loss spectroscopy (EELS) signal from Iron (Fe-L edge of 721 eV) was acquired in energy-filtered TEM (EFTEM) mode for the distribution of Fe phases in the samples. Elemental mapping was obtained by using a three-window method.

RESULT AND DISCUSSION

Synthesis of Oleic Acid (OA) Coated Iron Oxide Nanoparticles

The synthesis strategy was presented in Figure 1. The formation of iron oxide nanoparticle cores was accomplished by coprecipitation process, adding 1 : 2 ratio of Fe^{+2}/Fe^{+3} to an aqueous solution, maintained in an inert atmosphere at a high pH, which was obtained by addition of $NH_3{\cdot}OH$ solution. The different steps of modification were followed by chemical characterization (FTIR and TGA). The complete analysis is shown as Supporting Information (Figures S1–S3), demonstrating that polystyrene-functionalized nanoparticles were successfully obtained.

As shown in Figure 2, the pristine magnetic nanoparticles were examined by XRD, which represents patterns of iron oxide nanoparticles with six characteristic peaks of 2θ, 30.2 (220), 35.5 (311), 43.3 (400), 53.5 (422), 57.1 (511), and 62.6 (440), which are similar to the standard data for magnetite or maghemite, both spinel structures, which are ferrimagnetic.[18,19] Nanoparticles could also be formed by magnetite and partially oxidized to maghemite at their surface. The particle size of nanoparticles produced was 12.6 ± 1.0 nm, calculated using Debye-Scherrer formula,[20] from the XRD patterns.

$$D_{hkl} = k\lambda/\beta\cos\theta \quad (1)$$

In Debye-Scherrer formula shown above [eq. (1)], D_{hkl} is the average particle size parallel to the (hkl) plane, k is a geometrical constant with a typical value of 0.89 for spherical particles, λ is the wavelength of the radiation, β is the full width at half maximum (FWHM) in radians, and θ is the position of the diffraction peak. The six characteristic peaks were used for calculation to calculate an average value.

The oleic acid coated nanoparticles (OA-MNPs) were obtained in the same way as the pristine iron oxide nanoparticles, but using OA as surfactants. OA is widely used in nanoparticle synthesis because it can form a dense protective layer, which stabilizes nanoparticles. Thereby they are well dispersed in water and organic solvent without aggregation, which is essential to the further modification. Moreover, the oleic acid layer prevents the oxidation of nanoparticles by O_2. When adding salts like NaCl as inducer, they could transfer into toluene under the protection of single layer of OA. Salts were used to destroy the emulsion formed by free oleic acid and accelerate the separation of water and organic solvent. This method to produce oil soluble nanoparticles from water-soluble nanoparticles has been reported.[21]

The morphology of spherical oleic acid coated nanoparticles is confirmed by TEM [see Figure 3(a)]. The size of MNPs calculated by analyzing TEM image (Figure 3) is 12.9 nm, which is similar to crystallite size 13 nm determined by XRD. The electron diffraction pattern [inset in Figure 3(a)] indicates the high crystallinity of the nanoparticles. No big aggregates can be observed in TEM image of low magnification [Figure 3(a)]. It indicates that OA-MNPs can be well dispersed in toluene. The pristine nanoparticle size measured by TEM is around 11.8 nm (Supporting Information, Figure S6). This value is close to the nanoparticles coated by oleic acid (Figure 3). Also the morphology of single particles is the same, except that the particles strongly aggregate without oleic acid. It proves that during the coprecipitation step the addition of oleic acid did not change the size and morphology of nanoparticles significantly, but improved the dispersion of nanoparticles.

To complement the TEM images, which only provide information on the iron oxide cores, hydrodynamic diameter of oleic acid coated MNPs was measured by DLS. Figure 3(b) inset shows the narrow hydrodynamic size distribution of MNPs and average diameter of 18.9 nm. The difference of particle size between TEM and DLS results from two reasons. First in the TEM image (Figure 3), only the core of Fe_3O_4 can be observed, and the organic shell is not discernible due to the lack of contrast. DLS measures the total particle size, including the OA layers. A second factor comes from the difference of measuring environment in light scattering and TEM. Particles can swell and be surrounded by liquid shells in solvent during DLS measurements, while volumetric shrinkage may occur during drying in TEM sample preparation. Generally, DLS-measured particle sizes are larger than that imaged by transmission electron microscopy.[22]

The chemical analysis shown in the Supporting Information reveals that oleic acid is chemisorbed onto the iron oxide nanoparticles as a carboxylate ligand through chelating bidentate interaction.[23]

Thermogravimetric analysis was studied for pristine MNPs, OA-MNPs, NH_2-MNPs, Br-MNPs, PS-MNPs, and pure PS from room temperature to 1000°C under N_2 protection, as shown in Figure S2 in the Supporting Information. The TGA curve of pristine MNPs indicates that the weight loss of iron oxide can be neglected at high temperature up to 1000°C, which implies N_2 flow could prevent Fe_3O_4 from being oxidized to Fe_2O_3

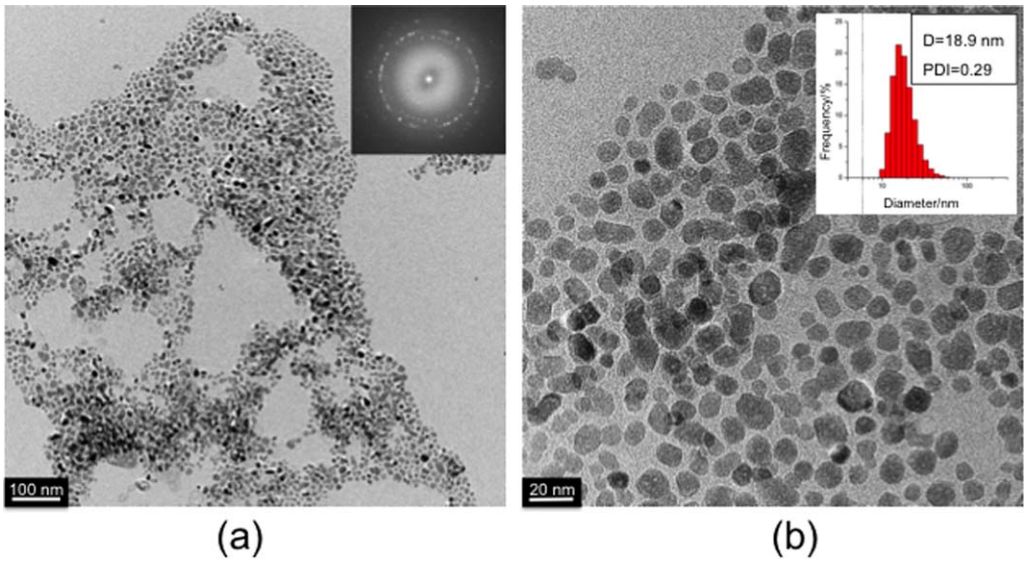

Figure 3. TEM images of OA coated iron oxide nanoparticles in toluene (a) low magnification, (b) high magnification, and the electron diffraction pattern (inset a); particle hydrodynamic size distribution measured by DLS (inset b). [Color figure can be viewed in the online issue, which is available at wileyonlinelibrary.com.]

effectively. The oleic acid content on the surface of nanoparticles was determined by TGA curve (b), which shows a final weight loss of about 38%. A two-step mass loss can be observed. The first continuous mass loss of about 7% was obtained from a temperature of 170 and 610°C. The second sharp mass loss of about 30% occurred between 720 and 880°C. Because organic compounds are supposed to be decomposed at 600°C, the first weight loss is attributed to the degradation of oleic acid coated on the nanoparticles. The second weight loss after 720°C may result from the reduction of Fe_3O_4 nanoparticles from magnetite to hematite by the reducing byproducts from the degradation of oleic acid.[24]

Synthesis of Initiator Coated Iron Oxide Nanoparticles

ATRP initiator coated iron oxide nanoparticles were synthesized as illustrated by Figure 1. Amino groups were first immobilized on the surfaces of the iron oxide core to obtain NH_2-MNPs via ligand-exchange between OA and APTES and condensation reaction between the hydroxyl groups on the MNPs and triethoxysilane groups of APTES. Second, the NH_2 groups on MNPs were further reacted with 2-bromoisobutyryl bromide (BiBB), leading to ATRP initiator Br-MNPs.

Morphology similar to that shown in Figure 3 for OA-MNPs was observed for the nanoparticles further coated with NH_2 and Br (Figure S7, Supporting Information). The diameters of the nanoparticle cores almost remained unchanged, but DLS measurement indicates the hydrodynamic diameter of MNPs was altered in the course of the functionalization process. The hydrodynamic diameter of the nanoparticles increased to 30.5 nm with incorporation of NH_2 groups, as shown in Figure S8, Supporting Information. But after immobilizing BiBB (Br-MNPs), the hydrodynamic diameter dropped to 18.9 nm, similar to OA-MNPs. This phenomenon implies that the polar amino group might lead to particle agglomeration, while the bromide as end group on the nanoparticle surface enabled MNPs to disperse well in toluene. Self-condensation of trialkoxysilane,[25] was not observed in Br-MNPs or in later stages of modification.

In Figure S2, Supporting Information MNPs after each stage of modification give their distinctive TGA curves, which provide indications of the amount of organic components on MNPs. Considering the SiO_2 ash remained in the residue after oxidation, the coating density of NH_2-MNPs and Br-MNPs can be estimated from TGA analysis and their molecular weight according to the following equation:

$$\text{Number of molecules per nm}^2 = \frac{W \times \rho_{Fe_3O_4} \times d \times N_A}{M \times (1-W) \times 6 \times 10^{21}} \quad (2)$$

where W is the total weight loss of sample, ρ_{Fe3O4} is the density of Fe_3O_4, N_A is Avogadro's constant, M is the molecular weight, d is the diameter of nanoparticles.[26] The results are summarized in the table below:

Table I lists the coating density of functionalized nanoparticles. It is estimated that the grafting density of amino group-coated MNPs (NH_2-MNPs) is about 12.9 molecules per nm^2. After the second step modification, the coating density of ATRP initiators on the surface of Br-MNPs is reduced to about 6.2 molecules/nm^2. This is probably because some APTES molecules on the surface of MNPs did not react with BiBB. By azeotropic distillation of water residues, the condensation reaction was driven to high conversions, yielding in a tight inter-crosslinked functional monolayer on the particle surface.[27]

Table I. Coating Density of Functionalized Iron Oxide Nanoparticles

Functionalized MNPs	Total weight loss (%)	Coating density (1/nm^2)
NH2-MNPs	10	12.9
Br-MNPs	16	6.2

Table II. Results from the GPC Analysis of Free PS and Cleaved PS

Sample	M_n (g/mol)	M_w (g/mol)	PDI	Weight loss (%)	Coating density (1/nm^2)
Free PS	9998	11,667	1.17	99	N/A
Cleaved PS	3215	8041	2.50	94	1.8

Surface Initiated ATRP of Styrene on Iron Oxide Nanoparticles

The bromine-terminated Br-MNPs were subsequently used for the copper-mediated ATRP of styrene without addition of free initiators (sacrificial initiators) to form iron oxide/polystyrene core/shell nanoparticles, as described in Figure 1. As a reference, free polystyrene was synthesized via conventional ATRP in the presence of CuBr/PMDETA complex as catalyst and (1-bromoethyl)benzene as initiator.

To determine the molecular weight of the tethered PS chains the iron oxide core was etched with sodium hydroxide and hydrochloric acid, and the cleaved polymer chains were characterized using GPC. The GPC traces of free polymer chains and are cleaved polymer chains from MNPs surface shown in Figure S4, Supporting Information. According to the GPC analysis, the molecular weight and polydispersity (PDI) of PS on the surface of nanoparticles and free PS were calculated and summarized in Table II. The total weight loss was determined by TGA analysis. The coating density was estimated by eq. (2). The low PDI ($M_w/M_n = 1.17$) of pure polystyrene synthesized without MNPs reflects a controlled/"living" polymerization, which is also supported by the sharp peak in Figure S4(a) indicating narrow molecular weight distribution. The value of M_w/M_n from cleaved polystyrene, 2.50 is considerably higher than that of pure free polystyrene. A broad peak (Figure S4b) indicates that the polymer brushes on the surface of nanoparticles have wider molecular weight distribution than that of nonlinked polystyrene. The higher polydispersity may reflect heterogeneity in the functionalization or irregular cleavage previous to the GPC analysis.

The morphology of iron oxide nanoparticles grafted with polystyrene is shown in Figure 4. After the surface was coated with PS, MNPs could be well dispersed in toluene. Nanoparticles were stabilized by steric repulsion of polystyrene chains in good solvent. Minimal aggregation can be observed in TEM picture for the nanoparticles coated with polystyrene, and the diameters of the nanoparticle cores almost remained unchanged. DLS measurement indicates that the average hydrodynamic diameter of PS-MNPs was 33.1 nm [Figure 4(b)], much higher than that of Br-MNPs. By assuming that no significant aggregation occurred, the growth of particle size can be assigned alone to the PS coating. The average thickness of PS shell is estimated to be around 20 nm. The successful grafting of polystyrene can be confirmed by the FTIR spectrum, as shown in Figure S5.

Iron oxide particles are known to be magnetic. To investigate their magnetization, a MPMS® SQUID VSM equipment was utilized. Figure 5 shows the magnetic hysteresis loops of as-synthesized pristine MNPs and functionalized MNPs at each stage including OA coated, amino and bromide terminated, and polystyrene grafted nanoparticles at room temperature in the field range of ±20,000 Oe. The first observation is that for all samples hysteresis loops and coercivity are almost negligible in the absence of an external magnetic field, suggesting that these as-synthesized magnetic nanoparticles possess superparamagnetic behavior at room temperature.[28] The reason for the superparamagnetism of MNPs is mainly that their size is so small that each particle is a single magnetic domain and the energy barrier for its spin reversal is easily overcome by thermal vibrations.[21] In our study, the diameter of MNPs core is about

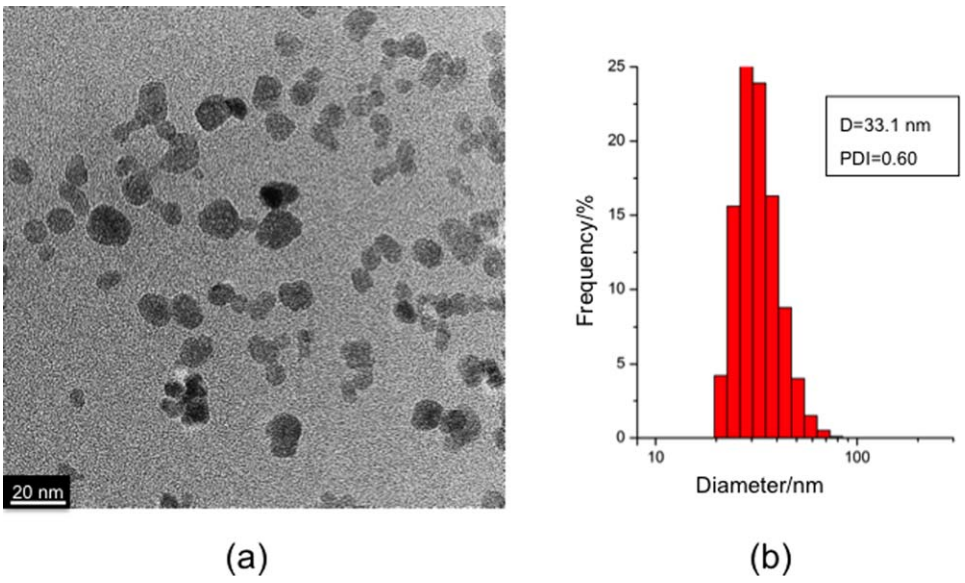

Figure 4. (a) TEM images of polystyrene coated iron oxide nanoparticles in toluene and (b) hydrodynamic size distribution determined by DLS. [Color figure can be viewed in the online issue, which is available at wileyonlinelibrary.com.]

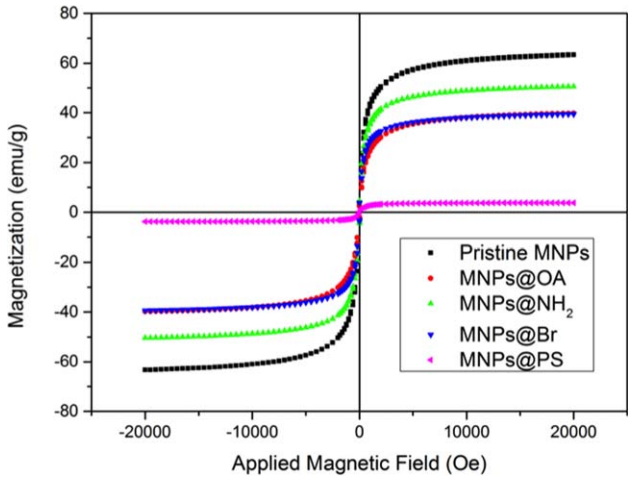

Figure 5. SQUID magnetic hysteresis loops for MNPs at different modification steps. [Color figure can be viewed in the online issue, which is available at wileyonlinelibrary.com.]

13 nm, which is less than 25 nm, the critical size of magnetite to exhibit superparamagnetism at room temperature based on the theoretical calculation.[29,30] Superparamagnetic nanoparticles do not retain any magnetism after removing the magnetic field. Residual magnetism would force nanoparticles to aggregate irreversibly, which is unfavorable for applications like targeted drug release.[31,32]

The saturation magnetization (Ms) value of the MNPs is listed in Table III. In the first column, the Ms values correspond to the whole samples including iron oxide and organic layers. By taking the percentage of iron oxide in the complex into account, the saturation magnetization can be normalized by the mass of iron oxide nanoparticles after subtracting the coating weight based on TGA results. The normalized Ms values in emu per mass unit of inorganic moieties are shown in the last column of Table III. As we can see, the saturation magnetization of the unmodified pristine iron oxide nanoparticles is about 63.4 emu/g at room temperature, which is consistent with the value reported by other researchers.[23,33] The Ms value of OA-MNPs

Table III. Saturation Magnetization of Iron Oxide Nanoparticles

Sample	Ms (emu/g sample)	% Iron oxide	Normalized Ms (emu/g iron oxide)
Pristine MNPs	63.4	98.5	64.4
OA-MNPs	39.8	62.2	64.0
NH_2-MNPs	50.6	90.6	55.8
Br-MNPs	39.4	84.1	46.8
PS-MNPs (membrane)	3.7	6.5	56.9

decreases significantly but the normalized Ms is almost identical to pristine MNPs, implying that the reduced Ms is due to the low content of iron oxide in the mixture diluted by oleic acid, while the magnetic property of the magnetite core was not sacrificed after surfactant coating. As to initiator coated MNPs, it can be observed that the normalized saturation magnetization of NH_2-MNPs and Br-MNPs drops to 55.8 and 46.8 emu/g, successively, which indicates that the covalently bonded silica monolayer, which was highly packed on the MNPs surface could affect the magnetic property considerably. The existence of PS grafted onto the surface of the iron oxide nanoparticles results in a low Ms of PS-MNPs, 3.7 emu/g. But if the content of iron oxide is taken in account and normalized, Ms rises to 56.9 emu/g, which is close to the values of nanoparticles from previous functionalization steps.

Preparation of Asymmetric PS-MNPs Films

Commercial ultrafiltration porous polymeric membranes are prepared by solution casting and phase inversion in water. By changing the polymer environment from a relatively good solvent to a nonsolvent, phase separation is initiated to different extents in different depths from the solution-water interface.[34] An asymmetric porous structure is obtained. Gelation/solidification of the phase separating system freezes the morphology in a state out of equilibrium. By changing the solvent mixture polymer composition and concentration a variety of morphology

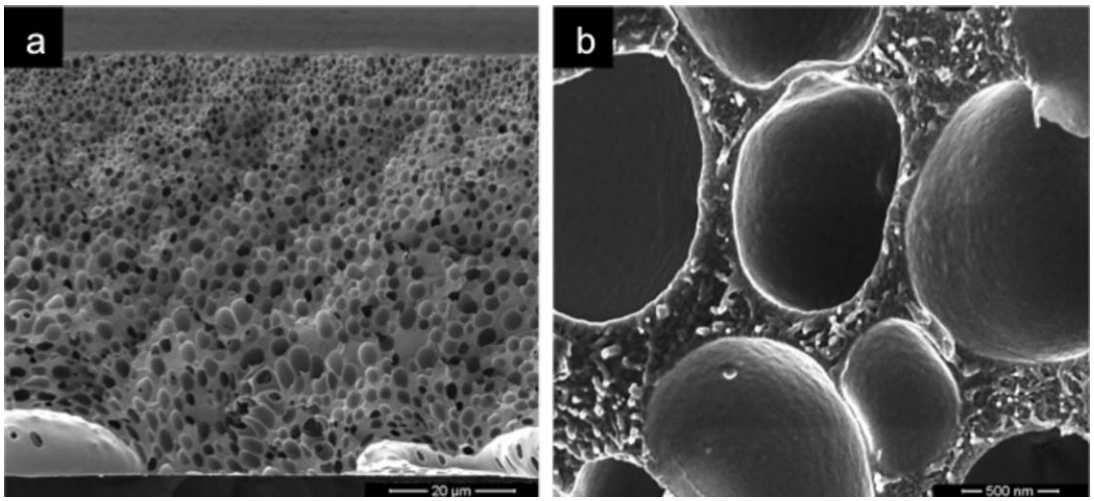

Figure 6. Cross-sections of the asymmetric PS-MNPs nanocomposite films 50 wt % in DMF (membrane A) at (a) low and (b) high magnifications.

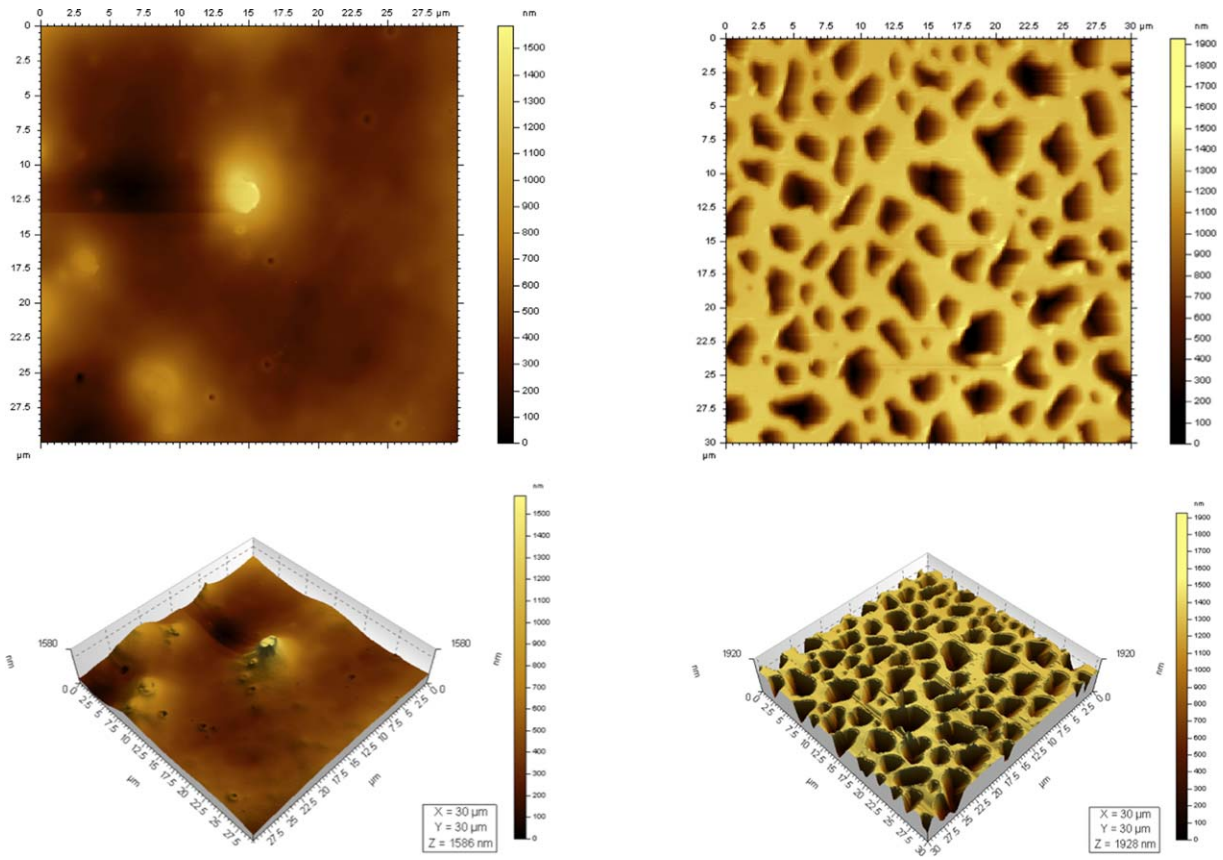

Figure 7. AFM images of the film surface of the PS-MNPs nanocomposite film prepared from 50 wt % casting solution: topological images of (a, b) top and (c, d) bottom. [Color figure can be viewed in the online issue, which is available at wileyonlinelibrary.com.]

can be obtained. When amphiphilic block copolymers are used instead of homopolymers, the self-assembly of block copolymer spherical micelles induces particular order and leads to the formation of isoporous surface layers.[16,17] We adopted an analogous procedure to produce asymmetric nanoparticle superlattices. We chose 2 different nanoparticles concentrations and investigated the morphology of the manufactured films. First films of about 100 μm thickness (membrane A) were cast from solutions containing 50 wt % PS-MNPs in DMF with the evaporation time of 25 s at room temperature. The solution layer was immersed in a water bath. Like for the membrane preparation processes with homopolymers and block copolymers, an asymmetric porous structure was immediately formed, with a gradient of nanoparticle concentration. The morphology is shown in Figures 6–8.

Figure 6 shows the FESEM images of cross-sections of the PS-MNPs nanocomposite films. The size of cavities near the surface is 1.1 ± 0.2 μm, while the size of cavities on the bottom side is 3.0 ± 0.5 μm.

The film surfaces (top and bottom) was investigated by AFM microscopy as shown in Figure 7. The images of the two sides reflect the porosity differences, the top layer (Ra = 22.7 nm) being smooth as compared to the highly porous opposite side (Ra = 249 nm).

The nanoparticle cores and their distribution could however be only imaged by TEM, as shown in Figure 8. The samples were embedded in epoxy resin, cut and imaged. Figure 8(a) is an overview of the membrane cross-section. The image is formed by elastic electrons. Darker regions in Figure 8(b,c) (higher magnification of 8a) correspond to the iron oxide cores. This is confirmed by the inelastic image, energy specific for Fe, shown in Figure 8(d) for the same region depicted in Figure 8(c). Now bright spots are rich in Fe.

Figure 9 shows now the morphology of nanocomposite films manufactured from 13 wt % nanoparticle solutions. Because of the low volatility of the solvents used, evaporation times of 0 to 25 s are practically equivalent and should not lead to changes in the incipient membrane top layer. By choosing the lower concentration of cast solution we achieved much more porous structure. The assembly of spherical polystyrene coated iron oxide nanoparticles can be clearly observed on the surface SEM. The surface roughness became higher than compared for films prepared with more concentrated casting solutions. The cross-section picture displays finger-like macrovoids below a thin top layer, and the loose pore walls consisted of MNPs@PS nanoparticles. It confirms that the assembly of nanoparticles at lower concentration led to highly porous structure not only on the surface, but also the interior of membrane.

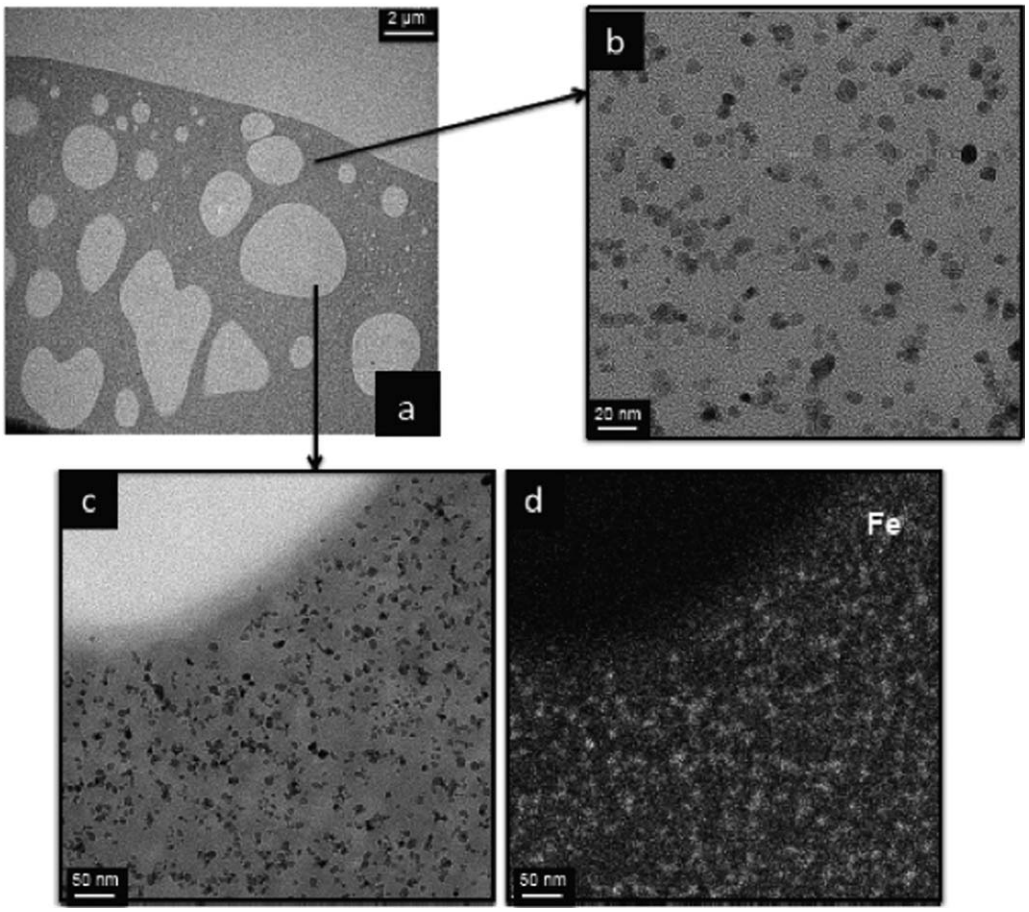

Figure 8. TEM images of the cross-sectional morphology of the PS-MNPs film prepared from 50 wt % casting solution: (a–c) elastic electrons image at different magnifications and (d) inelastic electron image specific for Fe (bright spots) of the same region of (c).

The above characterization of the as-fabricated PS-MNPs nanocomposite porous films demonstrate that the iron oxide particles are homogenenously distributed, separated from each other by the polystyrene shells. Segments of different shells entangle to form a self-standing film. A controlled gradient of magnetic particles is provided by the asymmetric porosity. Different casting condition gives different morphology of nanocomposite membrane, which widens the door for potential applications.

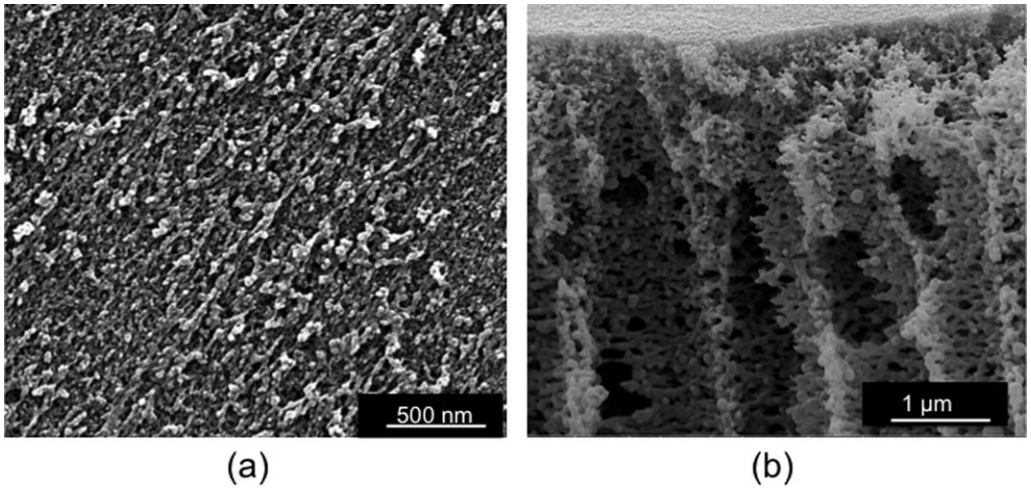

Figure 9. (a) Surface and (b) and cross-section of the asymmetric PS-MNPs nanocomposite films prepared from 13 wt % casting solution in NMP.

CONCLUSION

Asymmetric iron oxide/polystyrene hybrid films with controlled nanoparticles and porosity gradient were manufactured by phase inversion. Nanoparticles with ~13 nm diameter were prepared by coprecipitation in aqueous solution and modified with oleic acid. An initiator for ATRP was covalently bonded onto the surface of magnetic nanoparticles by silanization of ϒ-aminopropyl triethoxysilane (APTES) onto the surface and then esterification with the initiator, 2-bromoisobutyryl bromide (BiBB). ATRP of styrene was successfully carried out with a copper complex catalyst, Cu(I)Br-PMDETA. The following techniques, FTIR, EDAX, TEM, DLS, TGA, and VSM, were employed at different surface modification stages to confirm the successful surface functionalization. The molecular weight (M_n) of the tethered PS chains on nanoparticle surface was 3215 g/mol with a graft density of 1.8 molecules/nm^2. Fifty weight percentage PS-Fe_3O_4 nanoparticle solutions in DMF were cast and immersed in water, promoting phase inversion and forming a porous film with gradient concentration of Fe_3O_4 nanoparticles. The surface and cross-sectional morphologies of the membrane were examined by SEM, AFM, and TEM, demonstrating the porosity and particle distribution. Membranes cast from 13 wt % PS coated nanoparticle solution in NMP had higher porosity and finger-like cavities.

REFERENCES

1. Shipway, A. N.; Katz, E.; Willner, I. *ChemPhysChem.* **2000**, *1*, 18.
2. Xiong, S.; Dunphy, D. R.; Wilkinson, D. C.; Jiang, Z.; Strzalka, J.; Wang, J.; Su, Y. de Pablo, J. J.; Brinker, C. J. *Nano. Lett.* **2013**, *13*, 1041.
3. Lin, C. H.; Jiang, L.; Chai, Y. H.; Xiao, H.; Chen, S. J.; Tsai, H. L. *Appl. Phys. A* **2010**, *98*, 855.
4. Varon, M.; Beleggia, M.; Kasama, T.; Harrison, R. J.; Dunin-Borkowski, R. E.; Puntes, V. F.; Frandsen, C. *Sci. Rep.* **2013**, *3*, 1234.
5. Ohno, K.; Morinaga, T.; Koh, K.; Tsujii, Y.; Fukuda, T. *Macromolecules* **2005**, *38*, 2137.
6. Xu, C.; Ohno, K.; Ladmiral, V.; Composto, R. J. *Polymer* **2008**, *49*, 3568.
7. Xu, C.; Ohno, K.; Ladmiral, V., Milkie, D. E.; Kikkawa, J. M.; Composto, R. J. *Macromolecules* **2009**, *42*, 1219.
8. Harrison, R. J.; Dunin-Borkowski, R. E.; Putnis, A. *Proc. Natl. Acad. Sci. USA* **1999**, *26*, 16556.
9. La Conte, L.; Nitin, N.; Bao, G. *Mater. Today.* **2005**, *8*, 32.
10. Frenkel, J.; Dorfman, J. *Nature* **1930**, *126*, 274.
11. Nedkov, I.; Merodiiska, T.; Slavov, L.; Vandenberghe, R. E.; Kusano, Y.; Takada, J. *J. Magn. Magn. Mater.* **2006**, *300*, 358.
12. Wu, W.; He, Q.; Jiang, C. *Nanoscale Res. Lett.* **2008**, *3*, 397.
13. Laurent, S.; Forge, D.; Port, M.; Roch, A.; Robic, C. *Chem. Rev.* **2008**, *108*, 2064.
14. Tartaj, P.; Morales, M. P.; Veintemillas-Verdaguer, S.; Gonzales-Carreno, T.; Serna, C. J. *J. Phys. D: Appl. Phys.* **2003**, *36*, R182.
15. Zhou, L.; Yuan, J.; Wei, Y. *J. Mater. Chem.* **2011**, *21*, 2823.
16. Nunes, S. P.; Karunakaran, M.; Pradeep, N.; Behzad, A. R.; Hooghan, B.; Sougrat, R.; He, H.; Peinemann, K.-V. *Langmuir* **2011**, *27*, 10184.
17. Marques, D. S.; Vainio, U.; Chaparro, N. M.; Calo, V. M.; Bezahd, A. R.; Pitera, J. W.; Peinemann, K.-V.; Nunes, S. P. *Soft Matter.* **2013**, *9*, 5557.
18. Yang, T.; Shen, C.; Li, Z.; Zhang, H.; Xiao, C.; Chen, S.; Xu, Z.; Shi, D.; Li, J.; Gao, H. *J. Phys. Chem. B* **2005**, *109*, 23233.
19. Pichon, B. P.; Gerber, O.; Lefevre, C.; Florea, I.; Fleutot, S.; Baaziz, W.; Pauly, M.; Ohlmann, M.; Ulhaq, C.; Ersen, O.; Pierron-Bohnes, V.; Panissod, P.; Drillon, M.; Begin-Colin, S. *Chem. Mater.* **2011**, *23*, 2886.
20. Ge, J.; Hu, Y.; Biasini, M.; Dong, C.; Guo, J.; Beyermann, W. P.; Yin, Y. *Chem. Eur. J.* **2007**, *13*, 7153.
21. Wang, W.; Efrima, S.; Regev, O. *Langmuir* **1998**, *14*, 602.
22. Gittings, M. R.; Saville, D. A. *Colloids Surf. A: Phys. Eng. Aspects* **1998**, *141*, 111.
23. Sun, L.; Huang, C.; Gong, T.; Zhou, S. *Mater. Sci. Eng. C* **2010**, *30*, 583.
24. Yang, K.; Peng, H.; Wen, Y.; Li, N. *Appl. Surf. Sci.* **2010**, *256*, 3093.
25. Deng, Y.-H.; Wang, C.-C.; Hu, J.-H. ; Yang, W.-L.; Fu, S.-K. *Colloids Surf. A: Phys. Eng. Aspects* **2005**, *262*, 87.
26. Li, Q.; Zhang, L. F.; Zhang, Z. B.; Zhou, N. C.; Cheng, Z. P.; Zhu, X. L. *J. Polym. Sci. Part A: Polym. Chem.* **2010**, *48*, 2006.
27. Frickel, N.; Messing, R.; Gelbrich, T.; Schmidt, A. M. *Langmuir* **2010**, *26*, 2839.
28. Zhou, Y.; Wang, S.; Ding, B.; Yang, Z. *Chem. Eng. J.* **2008**, *138*, 578.
29. Chikazumi, S.; Taketomi, S.; Ukita, M.; Mizukami, M.; Miyajima, H.; Setogawa, M.; Kurihara, Y. *J. Magn. Magn. Mater.* **1987**, *65*, 245.
30. Meikiejohn, W. H. *Rev. Mod. Phys.* **1953**, *25*, 302.
31. Zhou, L.; Yuan, J.; Yu, W.; Sui, X.; Wu, S.; Li, Z.; Shen, D. *J. Magn. Magn. Mater.* **2009**, *321*, 2799.
32. Hu, F. X.; Neoh, K. G.; Kang, E. T. *Biomaterials* **2006**, *27*, 5725.
33. Liu, J.; He, H.; Zhang, L.; Zhang, Z.; Zhu, J.; Yuan, L.; Chen, H.; Cheng, Z.; Zhu, X. *Langmuir* **2011**, *27*, 12684.
34. Nunes, S. P.; T. Inoue. *J. Membr. Sci.* **1996**, *111*, 93.